# Design of composite SC walls to prevent perforation from missile impact

Jakob C. Bruhl [a, *], Amit H. Varma [b, 1], William H. Johnson [c, 2]

[a] U.S. Army and Purdue University, School of Civil Engineering, 550 Stadium Mall Drive, West Lafayette, IN 47907-2051, United States
[b] Purdue University, School of Civil Engineering, 550 Stadium Mall Drive, West Lafayette, IN 47907-2051, United States
[c] Bechtel Corporation, 5275 Westview Drive, Frederick, MD 21703, United States

## ABSTRACT

This paper presents a three-step method for designing steel plate composite (SC) walls subjected to missile impact. This method can be used to compute the minimum required steel plate thickness for SC walls to prevent perforation due to missile impact. The design method was verified using the complete experimental database of 130 SC wall missile impact tests compiled as part of this research. The design method compares favorably with the observations and results from the experimental database and can be used within its range of applicability to design SC walls to prevent missile perforation. The paper also presents the development and benchmarking of 3D finite element models for predicting the behavior and local failure of SC walls subjected to missile impact. The models were benchmarked using test results from the experimental database and results were used to confirm the failure mechanism of SC walls subjected to missile impact. The benchmarked models were used to conduct analytical parametric studies to expand the database, and further verify the design method. The numerical modeling approach is recommended for future research and design of specific SC wall configurations to resist design basis missiles.

Published by Elsevier Ltd.

## 1. Introduction

Steel plate reinforced concrete (SC) walls are efficient from fabrication, erection, and construction perspectives. They have been used effectively as primary and secondary shield walls in the third generation of nuclear power plants [1,2], and are being considered for the next generation of small modular reactors. It is important, therefore, that engineers have an accurate and convenient method to design SC walls for resisting missile impact.

There are important differences between SC and conventional reinforced concrete (RC) walls. As shown in Fig. 1, the internal reinforcing bars are replaced by external steel plates connected by tie bars; composite action is provided by headed stud anchors. The concrete between the plates is plain concrete, i.e., there are no reinforcing bars to restrain shrinkage or influence concrete behavior under impact loads. For SC walls, the term reinforcement

ratio refers to the ratio of the total steel plate thickness to the total depth of the section ($\rho = 2t_p/T$).

Empirical equations and design methodologies for preventing local failure of RC walls by perforation, scabbing, or penetration limit states have long been available. These equations were established during the 1940s for munitions projectiles and later extended and modified to include the effects of missile deformability [3] and low velocity projectiles [4]. The design limit state selected for RC walls depends on the required level of protection. Scabbing is the most commonly selected design limit state because of the risk of damage to internal equipment or personnel. Perforation may be the design limit state for structurally robust safety-related components that can withstand impact from spalled concrete. DOE-3014 [3] provides equations to determine RC wall thickness required to prevent the limit states of scabbing, penetration, or perforation as applicable.

The local failure mode of SC walls for missile impact differs slightly from that of RC walls because the rear (non-impact side) steel plate prevents scabbing of the concrete prior to perforation [5]. When subjected to missile impact, SC walls may undergo the following events sequentially: (i) missile penetration on front (impact) side, (ii) rear steel plate bulging, (iii) rear steel plate

* Corresponding author. Tel.: +1 808 292 3344.
 *E-mail addresses:* jbruhl@purdue.edu, jakob.bruhl@gmail.com (J.C. Bruhl), ahvarma@purdue.edu (A.H. Varma), whjohnson@bechtel.com (W.H. Johnson).
 [1] Tel.: +1 765 496 3419.
 [2] Tel.: +1 301 228 7747.

**Nomenclature**

| | |
|---|---|
| $A_c$ | projectile contact area, in$^2$ |
| $b$ | integration limit based on material properties of the steel plate |
| $c_i$ | crack width constants for bilinear concrete tension softening model |
| $d$ | equivalent diameter of projectile, inches |
| $D$ | average outer diameter of the engine casing or missile, inches |
| $E$ | modulus of elasticity of the steel plate, psi |
| $f_c'$ | concrete compressive strength, psi |
| $f_t$ | concrete tensile strength, psi |
| $f_y$ | yield strength of the steel plate, psi |
| $G_f$ | fracture energy of concrete, psi·inch |
| $L_{eff}$ | effective length of a finite element, inches |
| $K$ | coefficient depending on concrete compressive strength |
| $m$ | mass of the missile and the concrete plug, lb·sec$^2$/in |
| $n$ | strain hardening exponent |
| $N$ | missile shape factor |
| $r_1$ | minor radius of conical plug, inches |
| $r_2$ | major radius of conical plug, inches |
| $t_p$ | rear steel plate thickness, inches |
| $t_p^r$ | required rear steel plate thickness, inches |
| $T$ | total wall thickness, inches |
| $T_c$ | concrete wall thickness, inches |
| $V_{elem}$ | volume of a finite element, in$^3$ |
| $V_o$ | initial impact velocity of the missile prior to impact, ft/sec |
| $V_p$ | missile velocity that just initiates perforation, ft/sec |
| $V_r$ | residual velocity, ft/sec |
| $w_i$ | concrete crack width, inches |
| $W$ | total engine or missile weight, lbs |
| $W_{CP}$ | weight of the concrete plug, lbs |
| $x_c$ | penetration depth, inches |
| $\beta$ | statistical variation factor |
| $\alpha_p$ | perforation reduction factor |
| $\rho$ | reinforcement ratio |
| $\rho_c$ | weight density of concrete, lbs/in$^3$ |
| $\sigma_s$ | quasi-static true radial compressive stress, psi |
| $\theta$ | Conical plug angle, degrees |

splitting, and finally (iv) perforation of the entire thickness. The governing local failure mode for SC walls is perforation because the rear steel plate limits scabbing on the non-impact side.

The equations and design methodologies developed for RC have not been thoroughly evaluated for applicability to SC. This paper describes a method for designing SC walls to prevent local failure due to impact from a variety of missiles (i.e., tornado, hurricane, internally-generated such as from turbine fracture, or aircraft impact). This method differs from other suggested methods as it relies on a combination of physics-based and empirical equations to account for the perforation of the concrete and steel plates separately and accounts for the interaction between them.

## 2. Evaluating SC walls for local failure

Published standards include experimentally verified equations to calculate the required RC wall thickness to prevent local failure due to missile impact [3,6,7]. To apply these methods to SC walls,
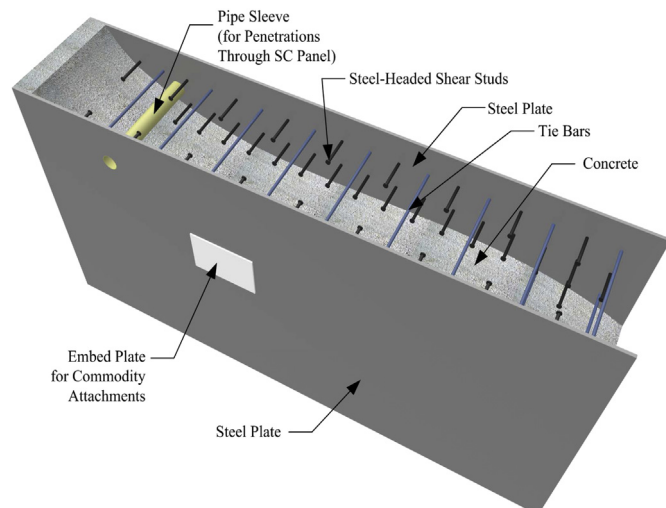


**Fig. 1.** Typical SC wall construction (from Ref. [35]).

some recommend converting the thickness of steel faceplates to equivalent thickness of concrete [8–10]. While the original equations in Refs. [8,9] are based on limited experimental data and do not account for the material properties of steel faceplates or their relation to the adjacent concrete, recent work expands this method to a wider range of parameters [10]. Mizuno et al. [11] published an empirical method, but it is limited to a single faceplate thickness and missile and does not account for material properties. There is a need for a general method that accounts for typical design parameters, accounts for the independent behavior of the concrete and steel portions of the wall, and follows the sequence of missile impact on SC walls.

### 2.1. Prior research and methods

Walter & Wolde [8] suggested that the steel faceplate thickness be considered as an equivalent concrete thickness, where the equivalence was calculated by equating perforation equations for steel plates to those for concrete slabs. This equation assumed concrete strength ($f_c'$) of 3800 psi, neglected the missile weight and diameter, and only considered the perforation limit state.

Tsubota et al. [9] presented equations to convert steel faceplate thickness to equivalent thickness of concrete perforation, splitting, and bulging limit states. The equations were developed empirically using results from a database of 50 experiments. The experiments supporting the development of these equations included panels with concrete strength of 3500 psi, thin steel sheets (0.03–0.08 in), and only one missile configuration. These equations are simple to use but limited in applicability.

Grisaro & Dancygier [10] expanded the work in Refs. [8,9] to convert steel plate to equivalent concrete across a range of concrete and steel strengths and missile weights and diameters. They developed their method using a best-fit approach by comparing different combinations of equations for the perforation velocity of concrete and steel. Their method is well-suited for assessing the perforation limit of existing structures but is not intuitive for use in design of new structures. Additionally, their approach focuses on conventional RC with a steel plate added for scabbing resistance rather than true SC walls without any additional reinforcement.

Mizuno et al. [11] provided a simple design tool in terms of a graph plotting the missile velocity with respect to the minimum wall thickness required to prevent the limit state of plate tearing (fracture). This graphical tool was developed for SC walls with 12 mm steel rear faceplates and one particularly large missile weight (44,000 lb).

## 2.2. Proposed three-step method for designing SC walls to resist perforation

An idealized failure mechanism, shown in Fig. 2, was used to develop a generalized method for designing SC walls to prevent the local failure of perforation for missile impact. This idealized mechanism was developed based on prior research (described above) and test results. As shown in Fig. 2 and demonstrated experimentally [5,9,15,23], the steel faceplate on the impact (front) side has little influence on the behavior with the exception that it constrains concrete spalling on its side. The missile can penetrate into the concrete thickness, and dislodge (fracture) a conical plug of concrete that starts moving at the same residual velocity ($V_r$) as the impacting missile. This conical concrete plug becomes the impacting projectile on the rear steel plate, and the rear steel plate must stop the mass of the concrete plug and original missile to prevent perforation (plate tearing/fracture) of the SC wall.

This paper presents: (1) the details of the generalized method and development of associated equations; (2) verification of the generalized method using the complete experimental database of SC wall missile impact tests; (3) development and benchmarking of 3D finite element models for predicting the local failure of SC walls subjected to missile impact; and (4) analytical parametric studies conducted to expand the experimental database, further verify the generalized method, and establish the range of parameters for which the generalized method can be used.

The generalized method for designing SC walls to resist local failure (perforation) due to missile impact consists of three steps:

Step 1. Selecting an initial concrete wall thickness, $T_c$, based on other design requirements or using 70% of the RC wall thickness calculated for missile resistance by the modified-NDRC equation [3,6].

Step 2. Computing the weight ($W_{CP}$) and residual velocity ($V_r$) of the concrete conical plug dislodged by the missile after penetrating into the SC wall, while considering reduction factors for engine deformability.

Step 3. Calculating the required thickness, $t_p^r$, of the rear steel faceplate to prevent its tearing fracture and thus perforation of the SC wall due to the concrete plug projectile.

## 2.3. Details of the three-step method

This generalized method can be used for a wide range of parameters. Several of the equations used in the development of this method are physics-based (i.e., developed based on energy balance or the theory of penetration), and can be applied beyond the experiments used to confirm their accuracy. Other equations incorporated in this method are empirical and the limits of their applicability are established so that the resulting method is not used for cases for which it may not be reasonable or accurate. Considering the envelope of applicability of all equations included, this method applies to the following range of parameters: (i) rigid and deformable missiles, (ii) initial missile velocity between 60 ft/sec and 750 ft/sec, (iii) no limit on missile weight, (iv) missile diameter smaller than or equal to twice the wall thickness, and (v) conventional steel and concrete construction materials.

### 2.3.1. STEP 1: select concrete wall thickness

The selected concrete wall thickness may be governed by an existing design or other design restrictions. For an existing design the procedure in this paper can be used to check or redesign it for missile impact resistance. If there are design restrictions, wall thickness can be selected to meet these restrictions and the procedure in this paper can be used to design the steel plate thickness required for missile impact. If there are no existing designs or restrictions the SC wall thickness can be estimated initially as 70% of the corresponding RC wall thickness determined using DOE-STD-3014 [3] or NEI 07-13 [6]. This recommendation is based on previous studies, which have shown that SC walls with 1–4% reinforcement have similar missile impact resistance as equivalent RC walls that are approximately 30% thicker [11].

### 2.3.2. STEP 2: estimate the weight and velocity of concrete plug

Fig. 2 shows the local failure mechanism associated with missile impact on SC walls. The missile is assumed to penetrate the concrete and dislodge a conical plug of concrete. Fig. 3 shows the dimensions assumed for the dislodged concrete plug. The missile and the concrete plug with weight equal to $W_{CP}$ and residual velocity $V_r$ become the projectile impacting the rear steel faceplate; the parameters of the missile impacting the rear steel plate now includes the concrete plug in front of the original missile. The residual velocity $V_r$ of the projectile is estimated using Equation (1), based on energy balance, which is provided in NEI 07-13 [6] (attributed to [16] and [17]). In Equation (1), $V_o$ is the original missile velocity and $V_p$ is the concrete wall perforation velocity required to dislodge the concrete conical plug. The weight of the concrete conical plug ejected by the missile is estimated using the plug geometry shown
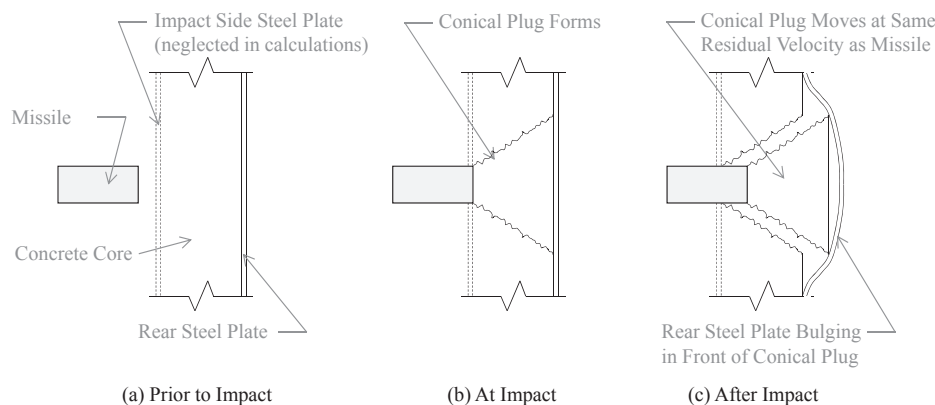


(a) Prior to Impact      (b) At Impact      (c) After Impact

**Fig. 2.** Impact sequence of missile on steel plate reinforced concrete wall.
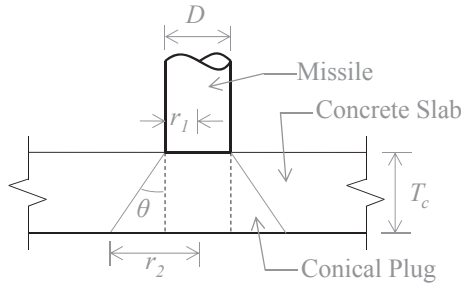
**Fig. 3.** Conical plug geometry (after [17]).

in Fig. 3 and Equations (2–4). This equation conservatively neglects the influence of tunneling of the missile into the wall, which would reduce the weight of the concrete plug and dissipate additional energy by concrete crushing. It is important to note that the failure mode assumed in Fig. 3 (the punching 'cone') is an idealization. Usually, at higher speed, the failure surface is more complex than that of the assumed idealized cone. There is some spalling (or scabbing in the back face) that is shallow, the failure surface may have a small theta angle, and the 'cone' may be almost a cylinder, depending on the speed, thickness of the slab, and diameter of the missile. This is based on observations of impact tests on RC walls [4,5]. These equations were developed for RC and may differ slightly when improved for SC walls.

$$V_r = \sqrt{\left\{\frac{1}{1 + W_{CP}/W}\right\}\left(V_o^2 - V_p^2\right)} \tag{1}$$

$$W_{CP} = \pi \rho_c \left(\frac{T_c}{3}\right)\left(r_1^2 + r_1 r_2 + r_2^2\right) \tag{2}$$

$$r_2 = r_1 + T_c \tan\theta \tag{3}$$

$$\theta = \frac{45°}{(T_c/D)^{1/3}} \tag{4}$$

The concrete wall perforation velocity ($V_p$) is computed using the procedure described in NEI 07-13 Section 2.1.2.4. Rather than doing this in multiple steps as NEI 07-13 describes, the equations were combined into individual equations to solve directly for $V_p$ (Equations (5)–(7)). These equations introduce a reduction factor, $\alpha_p$, which accounts for missile deformability (0.60 for deformable missiles, 1.0 for rigid missiles [6]). The equivalent diameter of the missile, $d$, can be calculated from the missile contact area, $A_c$, using Equation (8) [7]. For flat-nosed missiles, $d$ is equal to $D$. The two are also equal if there is a plate on the impacting end of a pipe. The strength coefficient, $K$, is calculated using Equation (9) and the missile shape factor, $N$, is 0.72 for flat-nosed, 0.84 for blunt-nosed, 1.0 for bullet-nosed, and 1.14 for sharp-nosed missiles. $N$ can be computed from Equation (10) for hollow missiles such as pipes [17]. If Equation (5) is the appropriate equation to use to compute the perforation velocity and the missile diameter is less than 5.9 in, then $N$ is to be taken equal to 1.14 regardless of the nose shape [6].

$$V_p = 1000 \cdot d \left(\frac{d}{1.44 K \cdot W \cdot N \cdot \beta^2}\left(2.2 \pm \sqrt{4.84 - 1.2\left(\frac{T_c}{\alpha_p d}\right)}\right)^2\right)^{5/9}$$

$$\text{for} \quad \frac{T_c}{\alpha_p d} \leq 2.65 \tag{5}$$

$$V_p = 1000 \cdot d \left(\frac{d}{4 K \cdot W \cdot N \cdot \beta^2}\left(\frac{T_c}{1.29 \alpha_p d} - 0.53\right)^2\right)^{5/9}$$

$$\text{for} \quad 2.65 < \frac{T_c}{\alpha_p d} < 3.27 \tag{6}$$

$$V_p = 1000 \cdot d \left[\frac{1}{K \cdot W \cdot N \cdot \beta}\left(\frac{T_c}{1.29 \alpha_p} - d(0.53 + \beta)\right)\right]^{5/9}$$

$$\text{for} \quad \frac{T_c}{\alpha_p d} \geq 3.27 \tag{7}$$

$$d = \sqrt{\frac{4A_c}{\pi}} \tag{8}$$

$$K = \frac{180}{\sqrt{f'_c}} \tag{9}$$

$$N_1 = 0.72 + \left(\left(\frac{D}{d}\right)^2 - 1\right)0.0306 \leq 1.0 \tag{10}$$

The factor $\beta$ was calculated from the statistical variation between the measured and calculated values of penetration depth from experimental results. This variation may be due to the fact that the modified-NDRC equations were developed for very thick targets while the specimens in the database are of limited thickness. Additionally, these tests include steel plates that are often interpreted to provide additional (equivalent) concrete thickness, which is not directly accounted for in the equation for penetration depth.

Section 3 presents the experimental database of relevant missile impact tests. These include 91 tests in which the missile was stopped by the composite wall. The missile penetration depth, $x_c$, was reported for 58 of these 91 tests. These 58 tests were used to evaluate the variation between the penetration depths calculated by the modified-NDRC equations, $x_{c(calc)}$, and those measured experimentally, $x_{c(test)}$. Statistical evaluation of these comparisons indicated that a multiplier, $\beta$, of 1.45 was needed for the calculated penetration depth to achieve a 5% probability of exceedance for the ratio of $x_{c(test)}$ to $x_{c(calc)}$. This statistical evaluation is illustrated graphically in Fig. 4, which shows the variation of $x_{c(test)}/x_{c(calc)}$ for the 58 specimens in descending order.

The factor, $\beta$, was added as a multiplier to the modified-NDRC equations for $x_c$ and carried through the mathematical
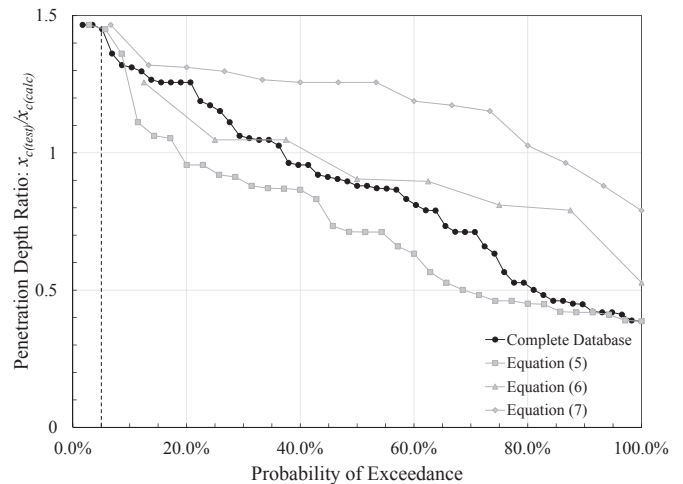


**Fig. 4.** Penetration depth probability of exceedance analysis.

development of the equations for $V_p$. $\beta$ appears in slightly different locations in Equations (5–7) because their forms and ranges are slightly different. Fig. 4 also includes the ratios of $x_{c(\text{test})}/x_{c(\text{calc})}$ for the three ranges in Equations (5–7). It confirms that the value of $\beta$ does not vary significantly between the three ranges. $\beta$ of 1.45 is recommended and used for further calculations in the paper. It is important to note that $\beta$ in Equations (5) and (6) has an influence of approximately $(1/1.45^2)^{5/9} = 0.65$ on the calculated value of $V_p$.

### 2.3.3. STEP 3: determine required rear steel plate thickness, $t_p^r$, to resist perforation

Børvik et al. [18] applied the plasticity concepts of cavity expansion and quasi-static radial stress to develop and verify equations to account for ductile metal plate perforation. These equations were rearranged as shown in Equation (11) to solve for the rear steel faceplate thickness, $t_p^r$, required to prevent its perforation due to the projectile impact. Børvik et al. used their equations to evaluate the perforation of aluminum plates but the equations were developed for strain hardening ductile metals impacted by missiles with a variety of nose shapes [19–21] and are therefore applicable for use in this design method. They are modified here to include the weight of the concrete plug (see Equation (12)) and the missile shape factor of 0.72 to account for the flat-nose of the concrete plug impacting the rear steel plate. The constant 12 in Equation (11) converts residual velocity from ft/sec to in/sec. The original missile diameter, $d$, is used in this calculation to account for the fact that a portion of the impacting concrete surface will crush and thus the entire diameter of the concrete plug does not impact the steel plate as a rigid projectile. The quasi-static radial compressive true stress, $\sigma_s$, is computed using Equation (13). In this equation, $n$ is the steel strain hardening exponent, and $b$ is the integration limit computed using Equation (14).

$$t_p^r = 0.72 \left( \frac{(12V_r)^2 m}{\frac{\pi}{2} d^2 \sigma_s} \right) \tag{11}$$

$$m = \frac{W + W_{CP}}{386 \text{in}/s^2} \tag{12}$$

$$\sigma_s = \frac{f_y}{\sqrt{3}} \left( 1 + \left( \frac{E}{\sqrt{3} f_y} \right)^n \int_0^b \frac{(-\ln(x))^n}{1-x} dx \right) \tag{13}$$

$$b = 1 - \frac{\sqrt{3} f_y}{E} \tag{14}$$

For structural steel plates, Equation (13) can be simplified to a linear equation in terms of the steel yield stress $f_y$. Equation (15) was developed using a modulus of elasticity of 29,000 ksi and strain hardening exponent ($n$) of 0.20 for plate steels. The strain hardening exponent has significant influence on the calculation of $\sigma_s$. Steel sheets with thickness less than 0.25 in, which are commonly used in scaled experimental specimens, exhibit very little strain hardening ($n$ values between 0.08–0.10 are common). As a result, Equation (15) will provide unconservative results when evaluating scaled tests using steel faceplates with thickness less than 0.25 in, and Equation (16) with strain hardening exponent $n$ equal to 0.10 is recommended instead.

$$\sigma_s = 5.1 f_y + 101000 \tag{15}$$

$$\sigma_s = 3.9 f_y + 64000 \tag{16}$$

## 3. Comparison with experimental results

A comprehensive database of missile impact tests performed on SC walls was compiled as part of this research. It included results from 130 missile impact tests conducted on SC walls by researchers over three decades [5, 8, 9, 14, 15, 22, and 23]. The tests summarized by Walter and Wolde [8], and those conducted by Sugano et al. [14] focused on RC walls, but included a few samples of RC walls with rear steel plates. Tests conducted by Abdel-Kader & Fouda [23], Barr et al. [15], Hashimoto et al. [5], Mizuno et al. [22], and Tsubota et al. [9] focused on SC walls with a few companion RC or plain concrete wall tests. Only SC wall specimens were included in this comparison.

The SC wall tests in the experimental database had a wide range of specimen and missile parameters. Missile weight ranged from 1.0 to 4600 lb; missile initial velocity ranged from 380 to 1400 ft/s; and missile diameter ranged from 0.9 to 39 in. SC wall thickness ranged from 2.0 to 54 in.; steel faceplate thickness ranged from 0.02 to 0.38 in.; concrete strengths ranged from 3000 to 7300 psi; and steel yield strengths ranged from 44 to 79 ksi. Of the 130 SC wall tests in the database: 91 specimens stopped the missile without perforating (or fracturing) the rear steel plate; and 39 specimens were perforated (with rear steel plate fracture) by the missile. 39 of the 130 tests (30%) have at least one parameter outside of the range of applicability of the design method (as described in Section 2.3). For comparative purposes and to determine if this method can reasonably be extended beyond the range of applicability from the equations which informed the method, these 39 tests were included in the following discussion.

The missile impact design procedure described in Section 2.0 was verified using the experimental database as follows. For each test specimen, the design procedure was used to calculate the rear steel plate thickness required ($t_p^r$) to prevent perforation. For cases where the actual or provided steel plate thickness ($t_p$) of the specimen was larger than 0.25 in. Equation (15) was used for the calculation of $\sigma_s$. Equation (16) was used for all other cases, where steel sheets with $t_p$ less than 0.25 in. were used for the specimens. If $t_p$ of the test specimen was greater than or equal to $t_p^r$, then it was expected to stop the missile without perforating the rear steel plate; if $t_p$ was less $t_p^r$, then the missile was expected to perforate the SC wall and fracture the rear steel plate. The design method was verified by comparing the expected outcome for each of the SC wall specimens in the experimental database to the observed outcome of each test. The numerical comparisons for all 130 specimens are provided as Supplemental Data to this paper, and discussed in more detail in the following sub-sections.

### 3.1. Tests in which specimens stopped the missile

91 specimens stopped the missile without perforating (or fracturing) the rear steel plate. Fig. 5 (a) shows comparisons of $t_p^r$ calculated by the design method with $t_p$ provided in the specimens. Of the 91 specimens, 30 had $t_p$ greater than $t_p^r$, and performed as expected. These 30 cases are shown in the shaded region of Fig. 5(a). The remaining 61 specimens had $t_p$ less than $t_p^r$, but stopped the missile without perforation: this means the design method is conservative. Four specimens had much larger $t_p^r$ (15–20 times $t_p$), and they are not included in Fig. 5(a) for clarity of scale (i.e., if included, they dwarf the rest of the points in the Figure). These four tests are all from Ref. [14] and lie in the unshaded portion (i.e., conservative portion) of the comparison shown in the Figure.
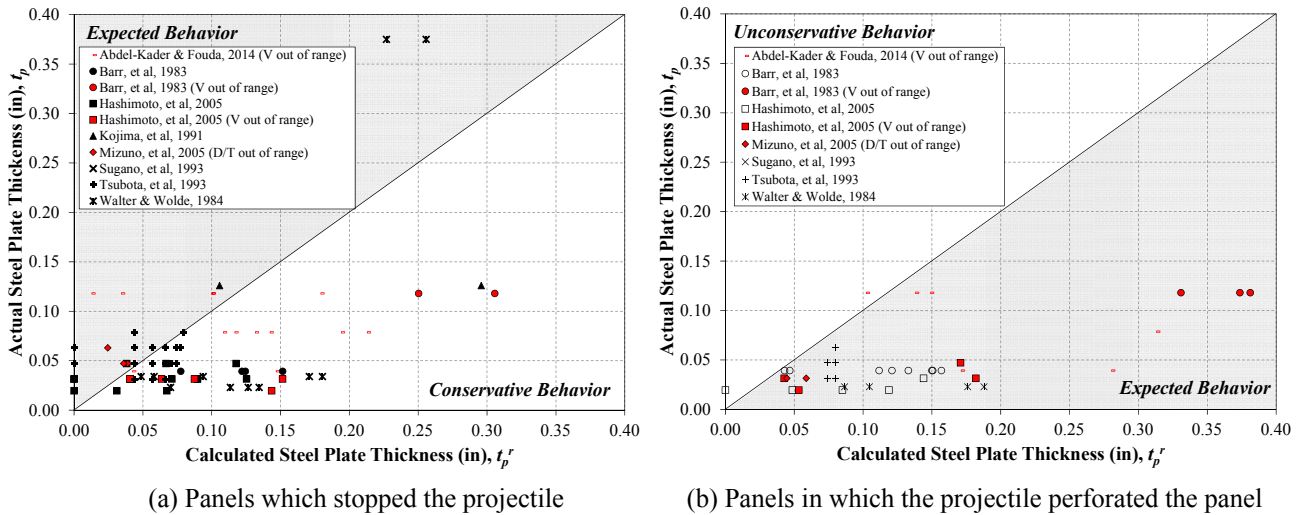
(a) Panels which stopped the projectile

(b) Panels in which the projectile perforated the panel

**Fig. 5.** Graphical comparison of calculated thickness to experimental tests.

### 3.2. Tests in which specimens were perforated by the missile

39 specimens were perforated (with rear steel plate fracture) by the missile impact. Fig. 5(b) shows comparisons of $t_p^r$ with $t_p$. As shown in the shaded region of Fig. 5(b), 37 specimens had $t_p$ less than $t_p^r$, and performed as expected, i.e., they were perforated. Two specimens had $t_p$ greater than $t_p^r$, but was still perforated by the missile, which is unconservative. One of these two tests is from Abdel-Kader & Fouda's tests [23] and the missile velocity falls outside of the range of applicability of this design method. The other unconservative test result was from Hashimoto's experiments [5] which were conducted on very small specimens (3 in thick SC walls and 1.8 in diameter missiles). For this test, the equations for RC walls suggest the concrete alone should have stopped the missile. One specimen from Ref. [14] had much larger $t_p^r$ (~30 times $t_p$) and is not included in Fig. 5(b) for clarity of scale. This test lies in the shaded portion of the comparison shown in the Figure, and performed as expected.

### 3.3. Summary of comparison with experimental results

In summary, the design method provides reasonable comparisons with experimental results. The results from the design procedure were as expected or conservative for 98% of the test results. In less than 2% of the cases (i.e., only two tests) the missile perforated SC walls with rear plate thickness ($t_p$) greater than or equal to $t_p^r$. This is a better comparison than either of the other three methods discussed in Section 2.1. Results from each of those methods are provided in Table 1 with specific results for each test provided in the Supplemental Data tables. This table presents the number of tests which fall into each category described in Section 3.1 and 3.2: those which stopped the missile and were conservative ($t_p$ less than $t_p^r$), which stopped the missile as expected ($t_p$ greater than or equal to $t_p^r$), those in which the missile perforated the wall as expected ($t_p$ less than $t_p^r$), and those which were perforated and were unconservative ($t_p$ greater than or equal to $t_p^r$). More conservative than results using the method in Refs. [10], the proposed method also provides the fewest unconservative results of the four methods.

Comparisons with the collected experimental results are important and useful, but limited in scope. The missile impact tests were conducted by a variety of researchers with differing objectives, and the resulting comparisons with the design method were

binary in nature, i.e., yes or no only. These comparisons confirmed the adequacy of the design method, but could not be used to further evaluate the missile impact behavior or performance of the SC wall specimens. The test specimens were not designed to confirm or evaluate rational design procedures nor were residual velocities of the perforating missiles reported for all tests in the database.

### 4. Numerical evaluation of missile resistance of SC walls

To better evaluate the accuracy of the design method, numerical models were developed using LS-DYNA [24] and benchmarked using tests from the experimental database. Sections 4.1 and 4.2 present additional details of FEM model development and benchmarking results. Section 4.3 presents results from the analytical parametric studies conducted using this benchmarked modeling method.

### 4.1. Benchmarking of numerical model

The FEM models were benchmarked using the tests conducted by Tsubota et al. [9], which were the most organized and comprehensive missile impact tests in the database. Tsubota's study systematically examined the influence of steel plates on the front and rear of reinforced concrete (RC) walls to improve impact protection of nuclear facilities from external missiles. They tested 50 SC wall (panel) specimens of varying concrete thickness and steel plate thickness. Each specimen was 23.6 in square with 0.24 in reinforcing bars at 3.94 in spacing as shown in Fig. 6. Eleven (11) of the fifty specimens had no steel plates — these RC panels served as the control specimens for the experimental program. Eight of the fifty specimens had steel plates attached with epoxy to the rear of the panel. The remaining 31 specimens (out of fifty) had plates

**Table 1**
Summary comparison of various methods to experimental database.

| Experimental result | Computed result | Walter & Wolde | Tsubota | Grisaro & Dancygier | | Proposed method |
|---|---|---|---|---|---|---|
| | | | | Ver. A | Ver. B | |
| Perforated | Unconservative | 36 | 31 | 9 | 10 | 2 |
| | Expected | 3 | 8 | 30 | 29 | 37 |
| Stopped | Conservative | 0 | 11 | 39 | 30 | 61 |
| | Expected | 91 | 80 | 52 | 61 | 30 |

0.24-in Φ deformed steel bars @3.94-in on-center

0.12-in Φ headed shear studs, 1.38-in long @1.97-in on-center

2.95-in

23.6-in

1.97-in

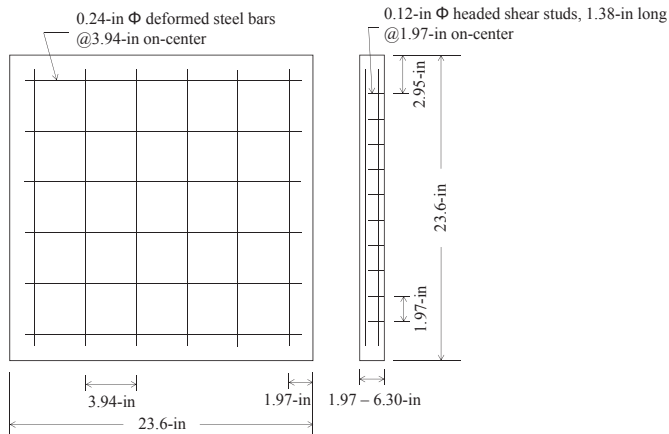3.94-in 1.97-in 1.97 – 6.30-in

23.6-in

**Fig. 6.** Tsubota et al.'s test panel design details.

attached with 0.12 in. diameter steel studs at 2 in. spacing: one specimen had steel plate on the impact side, one specimen had steel plates on both the impact and rear sides, and 29 specimens had steel plates only on the rear side. The missile mass, initial velocity, and concrete strength were constant for all tests.

As shown in Table 2, this modeling and benchmarking study included both RC and SC specimen tests. The models were developed using the geometric dimensions provided by Tsubota et al. and shown in Fig. 6. Reduced integration solid elements were used to model the concrete and steel plate(s). Beam elements were used to model the rebar and shear studs. Zero-length discrete beam (connector) elements were used to model the interfacial force-slip displacement behavior of the shear studs welded to the steel plate. All material input values used in this numerical analysis are provided in Tables 3–5.

### 4.1.1. Concrete material properties

The Winfrith concrete model (MAT_084/085) was developed in response to the nuclear industry's need to model accidental impact and blast loads on reinforced concrete structures and has been validated for a variety of impact and blast tests [25]. It is a smeared crack model that accounts for tension softening due to crack opening. The concrete compressive strength used in the models (3550 psi) was the measured value reported in the Tsubota et al.'s paper. The rest of the input parameters (elastic modulus, tensile strength, and fracture energy) were estimated using equations from accepted standards [26,27]. A bilinear curve is used to model tension softening (post-crack) concrete behavior as shown in Fig. 7 [28]. Crack widths ($w_1$ and $w_2$) associated with the points on the

**Table 2**
Panels modeled for benchmark study.

| Test# | Type | Face of liner | $T_c$ (in) | $t_p$ (in) |
|---|---|---|---|---|
| 1 | RC | None | 1.97 | 0 |
| 3 | RC | None | 2.76 | 0 |
| 7 | RC | None | 3.94 | 0 |
| 9 | RC | None | 4.72 | 0 |
| 14 | SC | Rear | 2.76 | 0.03 |
| 21 | SC | Rear | 1.97 | 0.05 |
| 24 | SC | Rear | 2.76 | 0.05 |
| 28 | SC | Rear | 3.94 | 0.05 |
| 29 | SC | Rear | 4.72 | 0.05 |
| 30 | SC | Rear | 1.97 | 0.06 |
| 39 | SC | Rear | 1.97 | 0.08 |
| 49 | SC | Front | 2.76 | 0.03 |
| 50 | SC | Both | 2.76 | 0.03 |

**Table 3**
Material properties for LS-DYNA models.

| | Benchmark | Analytical experiment |
|---|---|---|
| **Input for MAT_084 (concrete)** | | |
| Mass density, RO (lbf·sec$^2$/in) | $2.36 \times 10^{-4}$ | $2.36 \times 10^{-4}$ |
| Initial tangent modulus, TM (psi) | $3.40 \times 10^{6}$ | $4.0 \times 10^{6}$ |
| Poisson's ratio, PR | 0.15 | 0.15 |
| Uniaxial compressive strength, UCS (psi) | $3.55 \times 10^{3}$ | $5.0 \times 10^{3}$ |
| Uniaxial tensile strength, UTS (psi) | 237 | 141 |
| Fracture energy, FE (lbf·in/in$^2$) | 0.832 | 1.183 |
| Aggregate radius, ASIZE (in) | 0.125 | 0.375 |
| Rate effects (0 = ON, 1 = OFF) | 0 | 0 |
| Unit conversion, CONM | −1 | −1 |
| (−1 = lbf·sec/in2, in, sec) | | |
| **Input for MAT_ADD_EROSION (concrete)** | | |
| Erosion strain, MXEPS | 0.144 | 0.338 |
| **Input for MAT_003 (steel plate, rebar, and shear stud)** | | |
| Mass density, RO (lbf·sec$^2$/in) | $7.33 \times 10^{-4}$ | $7.33 \times 10^{-4}$ |
| Young's modulus, $E$ (psi) | $29.0 \times 10^{6}$ | $29.0 \times 10^{6}$ |
| Poisson's ratio, PR | 0.30 | 0.30 |
| Yield stress, SIGY (psi) | $77 \times 10^{3}$ | $64.5 \times 10^{3}$ |
| Tangent modulus, ETAN (psi) | $600 \times 10^{3}$ | $400 \times 10^{3}$ |
| Failure strain, FS (in/in) | 0.10 | 0.10 |
| **Input for MAT_068 (connector elements)** | | |
| Mass density, RO (lbf·sec$^2$/in) | $7.33 \times 10^{-4}$ | $7.33 \times 10^{-4}$ |
| Translational stiffness, TKR, TKS, and TKT (psi) | $29.0 \times 10^{6}$ | $29.0 \times 10^{6}$ |
| Rotational stiffness, RKR, RKS, and RKT (psi) | $11.0 \times 10^{6}$ | $11.0 \times 10^{6}$ |
| Load curve, LCPDR, LCPDS, and LCPDT | See Table 4; $Q_n = 639$ | See Table 4; $Q_n = 2870$ |
| Failure displ, UFAILR, UFAILS, and UFAILT (in) | 0.0445 | 0.084 |
| **Input for MAT_020 (rigid projectile)** | | |
| Mass density, RO (lbf·sec$^2$/in) | $6.60 \times 10^{-4}$ | See Table 5 |
| Young's modulus, $E$ (psi) | $29.0 \times 10^{6}$ | $29.0 \times 10^{6}$ |
| Poisson's ratio, PR | 0.30 | 0.30 |
| Constraints, CMO (0 = no constraints) | 0 | 0 |

**Table 4**
Load-slip curve for defining connector element behavior.

| Normalized load, $Q_i/Q_n$ | Slip, $\Delta_i$ (in) |
|---|---|
| 0 | 0 |
| 0.375 | 0.005 |
| 0.486 | 0.01 |
| 0.620 | 0.02 |
| 0.705 | 0.03 |
| 0.766 | 0.04 |
| 0.847 | 0.06 |
| 0.897 | 0.08 |
| 0.930 | 0.1 |
| 0.989 | 0.2 |
| 0.998 | 0.3 |
| 1.0 | 0.4 |
| 1.0 | 1.0 |

**Table 5**
Rigid projectile density based on missile diameter and weight (lb·sec$^2$/in).

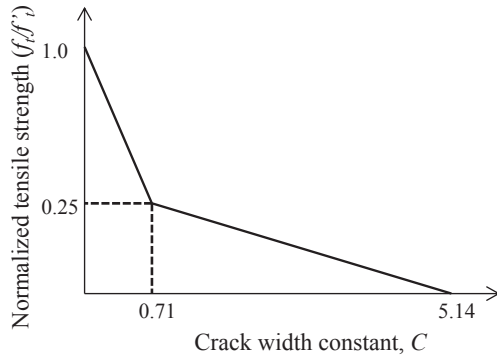| Missile weight (lb) | 6 in missile diameter |
|---|---|
| 10,000 | $5.09 \times 10^{-2}$ |
| 1000 | $5.09 \times 10^{-3}$ |
| 500 | $2.55 \times 10^{-3}$ |
| 200 | $1.02 \times 10^{-3}$ |
| 100 | $5.09 \times 10^{-4}$ |
| 60 | $3.06 \times 10^{-4}$ |
| 30 | $1.53 \times 10^{-4}$ |

**Fig. 7.** Bilinear tension softening model of Winfrith concrete model (after [28]).

bilinear curve are computed using Equation (17), in which $G_f$ and $f_t$ (UTS) are the fracture energy and tensile strength and $c_i$ is the crack width constant from Fig. 7.

$$w_i = c_i \frac{G_f}{f_t} \tag{17}$$

Careful consideration of the element erosion (deletion) criteria is important for conducting impact analysis. A maximum strain for concrete was set as the element erosion criteria using the keyword MAT_ADD_EROSION and was calculated as the maximum strain corresponding to the crack width ($w_2$) at zero residual tensile stress identified in Fig. 7. For the finite element mesh, the failure strain (MXEPS) was estimated using Equation (18), where $L_{eff}$ is the characteristic length of the concrete elements in the impact location estimated using Equation (19).

$$\text{MXEPS} = \frac{w_2}{L_{eff}} \tag{18}$$

$$L_{eff} = \sqrt[3]{V_{elem}} \tag{19}$$

When the crack grows to the maximum width, the tensile capacity becomes zero, and the element can be removed from the mesh. Table 3 lists the concrete material property input values for the finite element model (values not included in the table were left as default values).

### 4.1.2. Steel material properties

A bilinear kinematic hardening material model (MAT_003) was used for the rebar. No steel properties were measured or provided in Tsubota et al.'s paper, so Gr. 60 steel was assumed for the rebar, studs, and plate. Values for the Cowper-Symonds rate effects coefficients for steel vary widely in the literature, so dynamic increase factors were used as prescribed in NEI 07-13. The failure strain at which elements erode was set at 0.10. This is larger than the NEI 07-13 recommendation of 0.05 which is reasonable because the recommended failure strain is for design purposes focusing on fabricated (welded) steel plates and more conservative than behavior observed in small-scale tests. Table 3 lists the steel material property input values for the finite element model (values not included in the table were left as default values).

### 4.1.3. Shear studs

Shear studs can be modeled efficiently using beam and connector elements to account for the interfacial (pushout) force-slip displacement relationship [29]. The stud is modeled with beam elements with the same elasto-plastic kinematic hardening steel material model as the rebar. The shear stud (beam element) is embedded in the concrete (solid elements), and then connected to the steel plate with a zero-length connector (discrete beam) element. The connector element models the pushout force-slip displacement relationship developed by Olgaard et al. [30], confirmed experimentally by Anderson & Meinheit [31] and Shim et al. [32], and implemented analytically by Zhang et al. [29]. Table 4 provides the data points defining the normalized force-slip relationship for the studs in this model. As shown in Zhang et al., this modeling approach provides accurate force-slip displacement interaction between the steel plates and concrete infill of SC walls and also accounts for the interaction between the embedded stud and surrounding concrete.

### 4.1.4. Missiles

The missiles in Tsubota et al.'s tests were designed to be non-deformable, and were therefore modeled as rigid cylinders in LS-DYNA with 1.38 in. diameter and 2.36 in. length. The density was computed based on the known missile weight and the volume of the solid cylinder to ensure the missile mass was accurate. The material properties for the missile are listed in Table 3. Initial velocity as reported for each test was assigned to the rigid missile.

### 4.1.5. Other modeling details

The concrete was modeled using two different mesh densities: the central region in which the conical plug was expected to form consisted of 0.125 in. solid elements using constant stress reduced integration elements (SOLID ELFORM 1), and the outer region was composed of 0.5 in. solid elements with the same element formulation. The steel plate was modeled with the same mesh sizes as for concrete. The element formulation requires hourglass control, so Flanagan-Belytschko viscous form with exact volume integration for solid elements (IHQ3) was used with an hourglass coefficient of 0.10 as recommended by Erhart [33] for high-velocity analyses. Rebar was modeled with 0.5 in beam segments of Hughes-Liu with cross-section integration elements (BEAM ELFORM 1). The supports were modeled as 0.5 in diameter steel cables (using beam elements) embedded in the concrete at the top of the panel allowing the panel to swing upon impact as in the experiments.

Penalty based contact definition was used to define contact between the rigid missile and the SC walls and also to define contact between the steel plates and the concrete infill. Rebar, studs, and the support hangers were mathematically embedded in the concrete using a penalty coupling mechanism that assumes perfect bond with the concrete.

### 4.2. Benchmarking results

The results from the analytical models were compared with those published by Tsubota et al.'s and are summarized in Table 6. The results are reasonable for all cases, and in some cases are quite close to the experimental results. The damage mode in the numerical models is the same as that observed in all the tests. Figs. 8 and 9 show representative damage from the LS-DYNA analysis, which compare favorably with photographs of test specimens from Tsubota et al.'s experiments. Fig. 8 includes images of the front and rear faces of one of the specimens (Test 49) after impact. The experimental photos show similar damage to that obtained in the analysis including radial cracking and a conical crater. Fig. 9 shows the rear face of two other specimens (Test 1 and Test 50). Both are visually similar including bulging on the rear of one of the specimens (Test 50).

Fig. 10 shows contour plots of the maximum principle strains through the composite cross-section of three representative tests at the end of the computational runs. These plots show different

**Table 6**
Benchmarking model damage results comparison.

| Test# | Front crater diameter (in) | | Front crater depth (in) | | Rear bulge diameter (in) | | Rear bulge depth (in) | | Damage mode | |
|---|---|---|---|---|---|---|---|---|---|---|
| | Meas. | Model | Meas. | Model | Meas. | Model | Meas. | Model | Obs. | Model |
| 1 | 3.54 | 2.01 | N/A | N/A | N/A | N/A | N/A | N/A | Perf. | Perf. |
| 3 | 2.76 | 2.01 | N/A | N/A | N/A | N/A | N/A | N/A | Perf. | Perf. |
| 7 | 2.76 | 2.05 | 1.06 | 1.14 | N/A | N/A | N/A | N/A | Scab. | Scab. |
| 9 | 5.91 | 2.05 | 1.30 | 1.14 | N/A | N/A | N/A | N/A | Pen. | Pen. |
| 14 | 3.54 | 2.05 | 2.76 | 2.76 | 13.8 | 12.0 | 1.02 | 0.91 | Bulging | Bulging |
| 21 | 3.94 | 2.05 | N/A | N/A | 9.06 | 11.0 | N/A | N/A | Perf. | Perf. |
| 24 | 5.12 | 2.05 | 2.76 | 2.76 | 9.84 | 10.8 | 0.87 | 0.59 | Bulging | Bulging |
| 28 | 5.12 | 2.09 | 1.30 | 1.22 | 5.91 | 7.09 | 0 | 0.16 | Pen. | Pen. |
| 29 | 5.91 | 2.05 | 0.79 | 1.18 | 0 | 0 | 0 | 0 | Pen. | Pen. |
| 30 | 3.94 | 2.09 | 1.97 | 1.97 | 9.84 | 12.7 | N/A | 0.98 | Split | Split |
| 39 | 3.15 | 2.13 | 1.97 | 1.97 | 7.87 | 12.8 | 1.34 | 0.98 | Bulging | Bulging |
| 49 | 1.57 | 1.73 | N/A | N/A | 6.06 | N/A | N/A | N/A | Perf. | Perf. |
| 50 | 1.57 | 1.73 | 1.57 | 1.57 | 13.8 | 11.1 | 0.79 | 0.75 | Bulging | Bulging |

failure modes: (a) perforation, (b) rear steel plate bulging, and (c) penetration. Analyses were stopped after the missile came to rest or complete perforation had occurred. For clarity, the missile was removed from the images. The development of a conical concrete plug ahead of the missile is evident in each case. For cases where the conical plug completely separated from the surrounding concrete, but could not perforate the rear steel plate, the bulge of the rear steel plate formed by the front diameter of the plug is evident in the Figure.

The depth of the front crater was very similar for all cases. The same is not true for the diameter of the front crater in the tests without impact side steel plates because this modeling approach does not adequately capture concrete spalling on the impact side. For Tests 49 and 50, the diameter of the front crater was similar to that observed because of the presence of impact side steel plates, which prevented spalling on the impacted surface.

In all but two cases (Tests 14 and 50), the model predicted larger diameter bulges in the rear plate than those observed in the experimental tests. In both cases, the depth of the bulge was similar to that observed. In the other cases where perforation was prevented, the depths of the rear bulges were similar to those observed in the experiments.

To evaluate the accuracy of the method used to estimate the weight of the concrete conical plug dislodged, the size of the plug generated in the analysis was compared to the calculated values of the plug as described in Section 2.3.2. Fig. 10(a) indicates how the size of the concrete plug was measured from the numerical results. All but one plug from the numerical results were smaller than estimated as shown in Fig. 11. In this figure, the solid line is plotted using Equation (4) and the points are the measured plug angle, $\theta$, for the benchmark model cases. For those cases in which a plug was not completely formed, it was not possible to measure the major



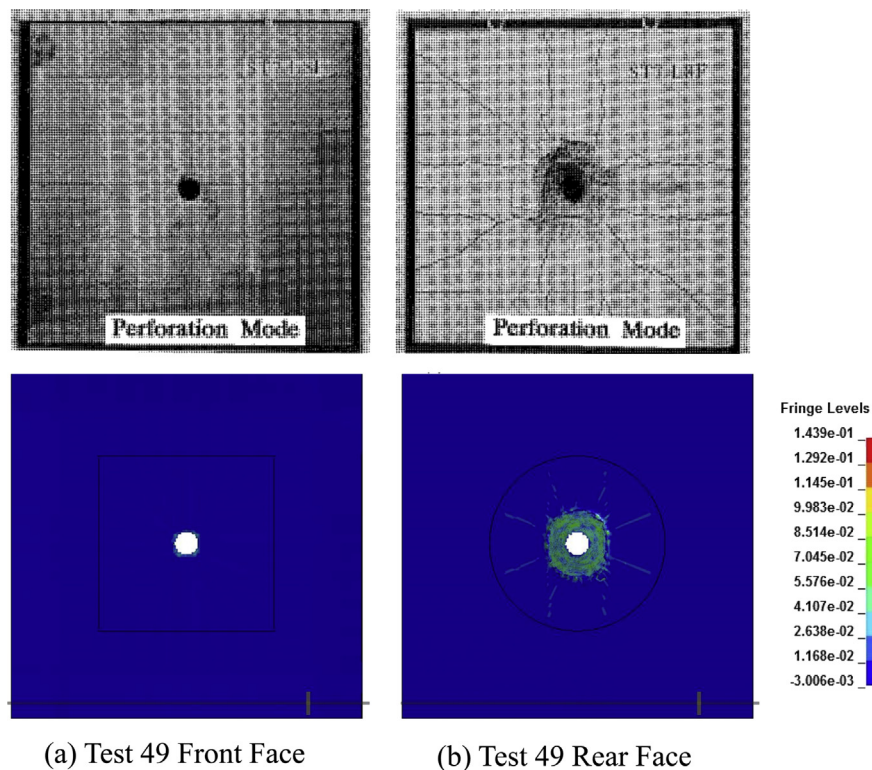(a) Test 49 Front Face    (b) Test 49 Rear Face

**Fig. 8.** Damage to test panel 49 in benchmarking study (fringe of maximum principal strain) [top images from Ref. [9] courtesy of IASMiRT at iasmirt.org].

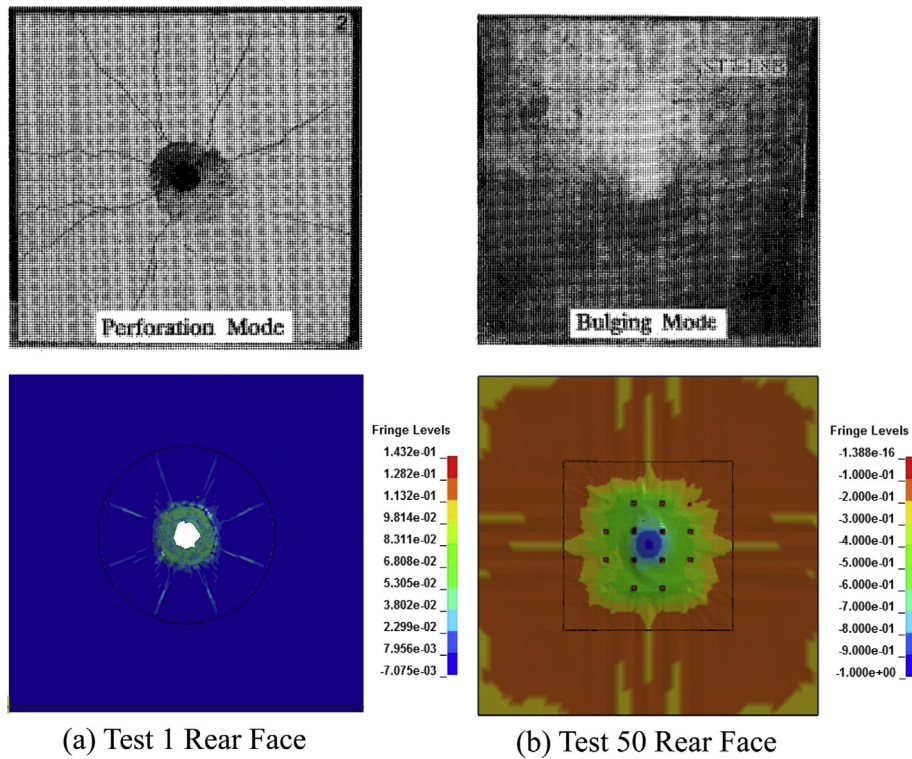(a) Test 1 Rear Face  (b) Test 50 Rear Face

**Fig. 9.** Damage to test panels 1 and 50 in benchmarking study (fringe of maximum principal strain) [top images from Ref. [9] courtesy of IASMiRT at iasmirt.org].

radius, $r_2$, in the model and thus three cases are not included in the Figure. On average, the plug angle was about 20% smaller than estimated which demonstrates that the method used to calculate the weight of the conical plug is conservative. It is likely that this reduction in plug angle is influenced by the steel plates. Preliminary analysis suggests the influence of changing the plug angle is minimal on the final design calculation but is an important aspect for future study of the mechanics of the idealized failure mechanism.

Importantly, these models validated the assumed failure mechanism described in Section 2.2. The impacting missile, penetrates the concrete, dislodges a conical concrete plug (if the velocity is high enough), and this plug and the original missile impact the rear steel plate which may bulge or fracture depending on the initial missile velocity. The modeling methods used for this benchmarking study are reasonable and slightly conservative and can therefore be used to conduct analytical parametric investigations of the local behavior of SC panels subjected to missile impact.

### 4.3. Parametric analysis of missile resistance of SC walls

To supplement the experimental database and further evaluate the performance of the missile impact design method presented in
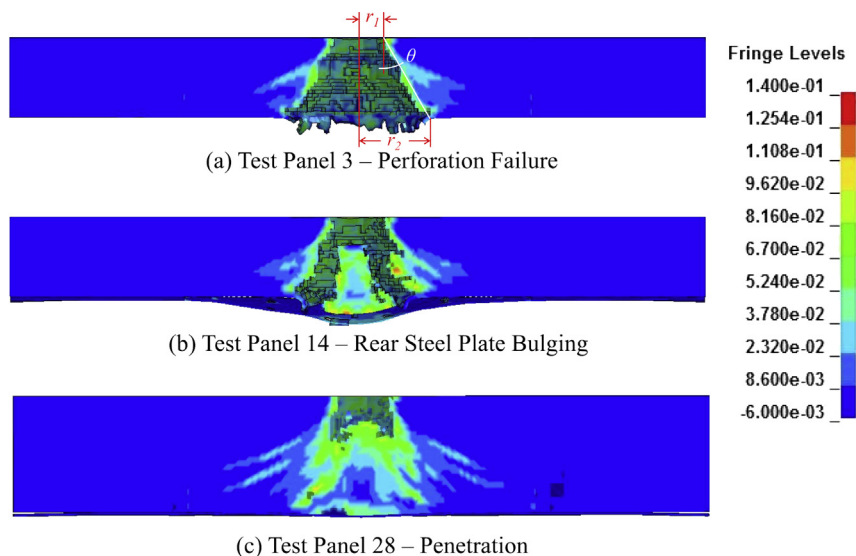


(a) Test Panel 3 – Perforation Failure

(b) Test Panel 14 – Rear Steel Plate Bulging

(c) Test Panel 28 – Penetration

**Fig. 10.** Representative failure modes from benchmarking study (fringe of maximum principal strain).
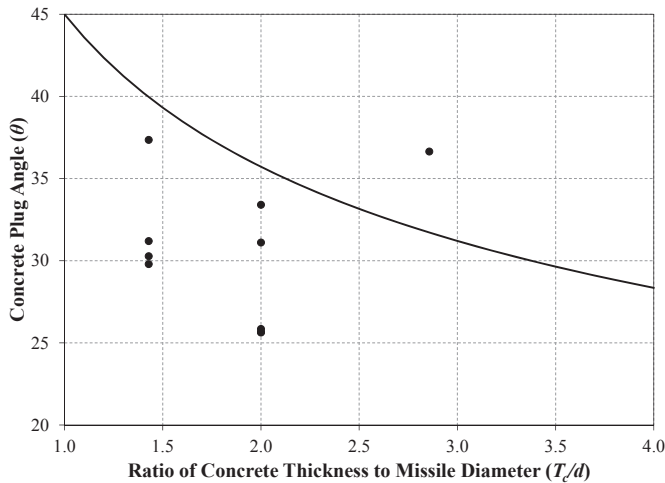
**Fig. 11.** Results of benchmarked model conical plug dimensions.

Section 3, analytical parametric studies were conducted using the benchmarked numerical modeling approach. The results of the parametric studies are presented in Table 7. The study focused on 6 in diameter rigid missiles impacting the minimum practical SC wall. Missiles of varying weight and initial velocity impacted numerical models of 12 in thick SC walls comprised of 0.25 in. thick steel plates resulting in a reinforcement ratio ($\rho = 2t_p/T$) of 4.2%. Several of these tests were beyond the range of applicable velocity for this design method. These cases were selected to evaluate if the design method could be extended to broader applicability.

### 4.3.1. Modeling details

The numerical models were analyzed using the benchmarked modeling approach described earlier. For computational efficiency, the models were axisymmetric: one-quarter of the SC wall was modeled with symmetric boundary conditions. Fixed boundary conditions were used for the edges to represent continuous walls.

The modeled SC walls had Gr-50 steel plates and concrete compressive strength of 5000 psi. Composite action was provided by 3 in. long 0.25 in. diameter shear studs spaced at 5 in. on-center. No tie bars were used in the models of the SC walls, which is a conservative assumption. The concrete mesh size in the central region (where the conical plug was expected to form) was 0.125 in, and the mesh size in the surrounding region was 0.50 in. The steel plate mesh size was uniform with 0.25 in. elements throughout. The missiles were modeled as 18 in. long rigid solid cylinders. Material properties for all components are listed in Tables 3—5

### 4.3.2. Parametric analysis results

Table 7 summarizes the results from the analytical parametric investigations. It includes comparisons of the analytical results with those calculated using the proposed three-step design method. The comparisons focus on the SC wall performance (perforation or stopping the missile), and the residual velocity of missiles perforating the SC wall model. As shown, the results from the numerical models compare well with the performance expected and calculated using the proposed design method. 16 of the 19 analyses performed as expected. Of the three tests that did not perform as expected, one was conservative, i.e., the calculated result from the design method was perforation, but the missile was stopped in the numerical analysis. This was for a case that had a higher velocity than the upper limit of applicability of this design method. The two tests that were unconservative were for an excessive missile weight of 10,000 lb at very low velocities (below the range of applicability of this design method). The calculations indicated that the SC wall should have stopped these missiles, but the numerical analysis results indicated perforation.

Fig. 12 compares the results from the numerical analysis with the results calculated using the proposed method. In the Figure, the line was developed using the three-step design method and shows the expected performance: for combinations of weight and velocity below the line, the SC wall is expected to stop the missile and for those above the line, the missile should perforate the SC wall. The red areas in the low- and high-velocity regions indicate the tests which were beyond the range of applicability of this design method. These results indicate that the minimum SC wall (12 in. thick with 0.25 in. thick steel plates) can safely resist perforation by the design basis tornado missile (schedule 40 pipe) and hurricane missiles as defined by Regulatory Guidelines (RG) 1.76 and 1.221 [12,13].

The results from this parametric study indicate that the proposed three-step method compares well with numerical analysis results for the range of applicability defined in Section 2.3.

**Table 7**
Analytical model combinations and results.

| Missile parameters | | | Result | | | Residual velocity (ft/sec) | |
|---|---|---|---|---|---|---|---|
| Diameter (in) | Weight (lb) | Initial velocity (ft/sec) | Modeled | Calculated | Agree? | Modeled | Calculated |
| 6 | 30 | 700 | Stop | Stop | Yes | 0 | 0 |
| 6 | 30 | 900 | Stop | Stop | Yes | 0 | 0 |
| 6 | 30 | 1100 | Stop | Perf. | No | 0 | 235 |
| 6 | 30 | 1500 | Perf. | Perf. | Yes | 463 | 456 |
| 6 | 60 | 450 | Stop | Stop | Yes | 0 | 0 |
| 6 | 60 | 600 | Stop | Stop | Yes | 0 | 0 |
| 6 | 60 | 700 | Perf. | Perf. | Yes | 134 | 149 |
| 6 | 100 | 400 | Stop | Stop | Yes | 0 | 0 |
| 6 | 100 | 500 | Perf. | Perf. | Yes | 138 | 71 |
| 6 | 200 | 250 | Stop | Stop | Yes | 0 | 0 |
| 6 | 200 | 350 | Perf. | Perf. | Yes | 152 | 66 |
| 6 | 200 | 450 | Perf. | Perf. | Yes | 252 | 217 |
| 6 | 500 | 150 | Stop | Stop | Yes | 0 | 0 |
| 6 | 500 | 250 | Perf. | Perf. | Yes | 168 | 117 |
| 6 | 1000 | 100 | Stop | Stop | Yes | 0 | 0 |
| 6 | 1000 | 200 | Perf. | Perf. | Yes | 152 | 126 |
| 6 | 10,000 | 30 | Perf. | Stop | No | 11 | 0 |
| 6 | 10,000 | 40 | Perf. | Stop | No | 26 | 0 |
| 6 | 10,000 | 50 | Perf. | Perf. | Yes | 38 | 23 |
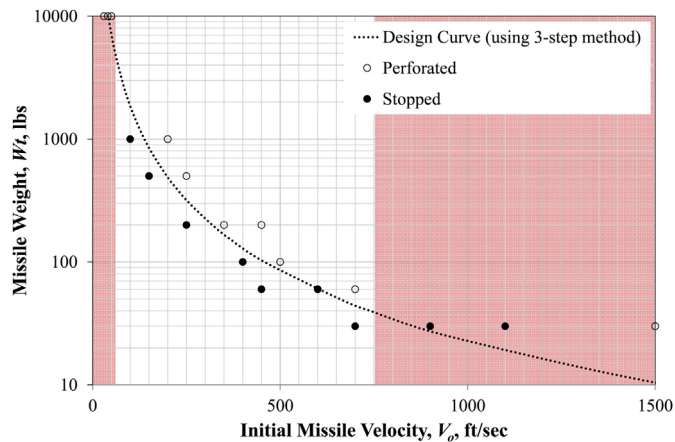
**Fig. 12.** Analytical tests compared to design curves (12 in thick wall; 0.25 in steel plates).

## 5. Design tools using three-step method

Recognizing the potential value of Mizuno's single design graph to practicing engineers, his approach can be extended to develop similar graphs that apply to a wide variety of wall and missile combinations. For example, to evaluate the resistance of a certain wall configuration, curves representing different missile diameters can be developed using the three-step method for given material properties. Similarly, curves for specific missile threats can be generated for walls with various reinforcement ratios to select the appropriate concrete thickness. Examples of such design tools are provided in AISC N690s1 [34].

## 6. Limitations and future work

The method presented in this paper designs an SC wall to prevent local failure. It does not consider the global response of the wall, which is discussed by the authors in a separate publication [35]. The SC wall may be able to prevent local perforation due to a particular missile, but it may still fail due to other impact design criteria such as flexural, shear, or deflection limits. Out-of-plane shear strength of SC panels is described in [36]. Additional research to determine deflection limits (e.g. ductility or rotation) of SC walls is necessary.

Additional research is recommended to further evaluate the influence of SC wall design parameters such as stud spacing, tie bar spacing, slenderness, and concrete and steel strength on missile impact behavior and local failure mode. The existing experimental database enables benchmarking of numerical models, which can be used to perform analytical parametric studies. It is recommended that future experimental work be conducted in coordination with numerical studies to further enhance and refine our understanding of SC wall performance subjected to impact loads. One aspect of these studies should be the influence of various design parameters on the size and shape of the conical plug formed in SC walls as compared to RC walls.

The tests used to validate the proposed method were from a variety of sources. They were conducted by different researchers with various purposes and objectives. They can only provide a binary check (pass or fail) for this design method. There is little insight into the accuracy of the method other than to say the SC wall panels in the tests performed as expected or not. Additional tests designed specifically to investigate the accuracy of the method are recommended. For example, a test of three panels, one with the plate thickness as calculated and the others with slightly thinner plates, would help demonstrate the conservatism of the method. Tests of multiple SC wall panels with the same dimensions subjected to missile velocity and weights above and below the design threshold would help evaluate sensitivity to those design parameters. Numerical studies can assist in this evaluation as shown in Section 4, but should be supplemented with experimental tests to ensure modeling methods are as realistic as possible.

## 7. Conclusions

There are currently no standardized methods for designing composite SC walls to resist missile impact. This paper presents a three-step method for designing SC walls subjected to missile impact. It can be used to compute the minimum required steel plate thickness for SC walls to prevent perforation from a realistic range of missile threats: initial velocities between 60 ft/sec and 750 ft/sec, diameters up to twice the panel thickness, and missile weights up to around 5000 lb. For parameters outside of this range, the detailed and benchmarked finite element analysis approach is recommended for conservative evaluation.

The design method was verified using the complete experimental database of SC wall missile impact tests compiled as part of this research. The design method compares favorably with the observations and results from the experimental database. For over 98% of the tests, the results were as expected or conservative with respect to the calculations from the design method. The two unconservative tests were conducted on extremely small-scale SC specimens.

The paper also presented the development of detailed 3D finite element models for predicting the behavior and local failure of SC walls subjected to missile impact. The models were benchmarked using test results from the experimental database, and used to confirm the failure mechanism used in the design method. The benchmarked models were used to conduct analytical parametric studies to expand the database, further verify the design method, and develop design tools along with their range of applicability for missile parameters.

The parametric studies indicated that the design method compares well with numerical analysis results for all cases within the defined range of applicability of the design method. The design tools and conclusions are applicable to the missile impacts of concern in the design of nuclear facilities including tornado, hurricane, internally-generated, and aircraft missile impact. The proposed method can be used confidently within its range of applicability to design for SC walls to prevent missile perforation.

## Appendix A. Supplementary data

Supplementary data related to this article can be found at http://dx.doi.org/10.1016/j.ijimpeng.2014.07.015.

## References

[1] DCD. Design control document for the US-APWR. Washington, D.C.: U.S. Nuclear Regulatory Commission; 2012. http://www.nrc.gov/reactors/new-reactors/design-cert/apwr.html.

[2] DCD. Design control document for the AP1000. Washington, D.C.: U.S. Nuclear Regulatory Commission; 2011. p. 1578. http://www.nrc.gov/reactors/new-reactors/design-cert/ap1000.html.

[3] U.S. Department of Energy. Accident analysis for aircraft crash into hazardous facilities (DOE-STD-3014). Washington, D.C.: U.S. Department of Energy; 2006. p. 215.

[4] Degen PP. Perforation of reinforced concrete slabs by rigid missiles. J Struct Eng ASCE 1980;106(7):1623–42.

[5] Hashimoto J, Takiguchi K, Nishimura K, Matsuzawa K, Tsutsui M, Ohashi Y, et al. Experimental study on behavior of RC panels covered with steel plates subjected to missile impact. In: Transactions of the 18th SMiRT. [Beijing, China]: International Association for Structural Mechanics in Reactor

Technology (IASMiRT); 2005. p. 2604–15. http://www.iasmirt.org/transactions/18/J05_4.pdf.

[6] Nuclear Energy Institute. Methodology for performing aircraft impact assessments for new plant designs (NEI 07-13 Revision 8P). Walnut Creek, CA: Nuclear Energy Institute; 2011. p. 69.

[7] American Society of Civil Engineers. Structural analysis and design of nuclear plant facilities (ASCE – manuals and reports on engineering practice – no. 58). New York, NY: American Society of Civil Engineers; 1980. p. 553.

[8] Walter TA, Wolde-Tinsae AM. Turbine missile perforation of reinforced concrete. J Struct Eng ASCE 1984;110(10):2439–55. http://dx.doi.org/10.1061/(ASCE)0733-9445(1984)110:10(2439).

[9] Tsubota H, Yasai Y, Noshika N, Morikawa H, Uchida T, Ohno T, et al. Quantitative studies on impact resistance of reinforced concrete panels with steel liners under impact loading part 1: scaled model impact tests. In: Transactions of the 12th SMiRT. [Stuttgart, Germany]: International Association for Structural Mechanics in Reactor Technology (IASMiRT); 1993. p. 169–74. http://www.iasmirt.org/transactions/12/J07-1.pdf.

[10] Grisaro H, Dancygier A. Assessment of the perforation limit of a composite RC barrier with a rear steel liner to impact of a non-deforming projectile. Int J Impact Eng 2014;64:122–36. http://dx.doi.org/10.1016/j.ijimpeng.2013.10.002.

[11] Mizuno J, Tanaka E, Nishimura I, Koshika N, Suzuki A, Mihara Y. Investigation on impact resistance of steel plate reinforced conrete barriers against aircraft impact part 3: analyses of full-scale aircraft impact. In: Transactions of the 18th SMiRT. [Beijing, China]: International Association for Structural Mechanics in Reactor Technology (IASMiRT); 2005. p. 2591–603. http://www.iasmirt.org/transactions/18/J05_3.pdf.

[12] U.S. Nuclear Regulatory Commission. Regulatory Guide 1.76, Revision 1, "Design-basis tornado and tornado missiles for nuclear power plants". Washington, D.C: U.S. Nuclear Regulatory Commission; 2007. p. 12.

[13] U.S. Nuclear Regulatory Commission. Regulatory Guide 1.221, "Design-basis hurricane and hurricane missiles for nuclear power plants". Washington, D.C.: U.S. Nuclear Regulatory Commission; 2011. p. 13.

[14] Sugano T, Tsubota H, Kasai Y. Local damage to reinforced concrete structures caused by impact of aircraft engine missiles, Part 1. Test program, method and results. Nuc Eng Des 1993;140:387–405. http://dx.doi.org/10.1016/0029-5493(93)90120-X.

[15] Barr P, Carter PG, Howe WD, Neilson AJ, Richards AE. Experimental studies of the impact resistance of steel faced concrete composites. In: Transactions of the 7th SMiRT. [Chicago, IL]: International Association for Structural Mechanics in Reactor Technology (IASMiRT); 1983. p. 395–402. http://www.iasmirt.org/transactions/07/J8-4.

[16] Sugano T, Tsubota H, Kasai Y. Local damage to reinforced concrete structures caused by impact of aircraft engine missiles, Part 2. Evaluation of test results. Nuc Eng Des 1993;140:407–23. http://dx.doi.org/10.1016/0029-5493(93)90121-O.

[17] Kar A. Residual velocity for projectiles. Nuc Eng Des 1979;53(1):87–95. http://dx.doi.org/10.1016/0029-5493(79)90042-6.

[18] Børvik T, Forrestal MJ, Hopperstad OS, Warren TL, Langseth M. Perforation of AA5083-H116 aluminium plates with conical-nose steel projectiles – calculations. Int J Impact Eng 2009;36(3):426–37. http://dx.doi.org/10.1016/j.ijimpeng.2008.02.004.

[19] Forrestal M, Luk V, Brar N. Perforation of aluminum armor plates with conical-nose projectiles. Mech Mater 1990;10(1–2):97–105.

[20] Forrestal M, Brar N, Luk V. Penetration of strain-hardening targets with rigid spherical-nose rods. J Appl Mech 1991;58:7–10.

[21] Forrestal M, Tzou D. Penetration into ductile metal targets with rigid spherical-nose rods. Int J Impact Eng 1995;16(5/6):699–710.

[22] Mizuno J, Sawamoto Y, Yamashita T, Koshika N, Niwa N, Suzuki A. Investigation on impact resistance of steel plate reinforced concrete barriers against aircraft impact part 1: test program and results. In: Transactions of the 18th SMiRT. [Beijing, China]: International Association for Structural Mechanics in Reactor Technology (IASMiRT); 2005. p. 2566–79. http://www.iasmirt.org/transactions/18/J05_1.pdf.

[23] Abdel-Kader M, Fouda A. Effect of reinforcement on the response of concrete panels to impact of hard projectiles. Int J Impact Eng 2014;63:1–17. http://dx.doi.org/10.1016/j.ijimpeng.2013.07.005.

[24] LSTC. LS-DYNA keyword user's manual V971, 2. Livermore, CA: Livermore Technology Software Corporation; 2012. p. 2994.

[25] SPD/D(95)363 Broadhouse BJ. Winfrith concrete model in LS-DYNA3D. AEA Technology; 1995. p. 17.

[26] American Concrete Institute. Building code requirements for structural concrete (ACI 318-11). Farmington Hills, MI: American Concrete Institute; 2011. p. 503.

[27] American Concrete Institute. Code requirements for nuclear safety-related concrete structures and commentary (ACI 349-06). Farmington Hills, MI: American Concrete Institute; 2006. p. 157.

[28] Schwer L. The Winfrith concrete model: beauty or beast? Insights into the Winfrith concrete model. In: 8th European LS-DYNA users conference. Strasbourg, France: Livermore Technology Software Corporation; 2011. http://www.dynalook.com/8th-european-ls-dyna-conference/session-12/Session12_Paper2.pdf.

[29] Zhang K, Varma H, Malushte S, Gallocher S. Effect of shear connectors on local buckling and composite action in steel concrete composite walls. Nuc Eng Des 2014;269:231–9. http://dx.doi.org/10.1016/j.nucengdes.2013.08.035.

[30] Ollgaard JG, Slutter RG, Fisher JW. Shear strength of stud connectors in lightweight and normal-weight concrete. AISC Eng J 1971:55–64.

[31] Anderson N, Meinheit D. Design criteria for headed stud groups in shear: part 1-Steel capacity and back edge effects. PCI J 2000;45(5):46–75.

[32] Shim CS, Lee PG, Yoon TY. Static behavior of large stud shear connectors. Eng Struct 2004;26(12):1853–60. http://dx.doi.org/10.1016/j.engstruct.2004.07.011.

[33] Erhart T. Review of solid element formulations in LS-DYNA. Stuttgart, Germany: LS-DYNA Forum 2011; 2011. p. 36.

[34] American Institute of Steel Construction. Specification for safety-related steel structures for nuclear facilities supplement No. 1 (AISC N690s1) PUBLIC REVIEW DRAFT DATED 5-1-14. Chicago, IL: American Institute of Steel Construction; 2014. p. 106.

[35] Johnson W, Bruhl J, Reigles D, Li J, Varma A. Missile impact on SC Walls: global response. Structures Congress 2014. Reston, VA: American Society of Civil Engineers; 2014. p. 1403–14. http://dx.doi.org/10.1061/9780784413357.124.

[36] Sener K, Varma A. Steel-plate composite walls: experimental database and design for out-of-plane shear. J Constr Steel Res 2014;100:197–210. http://dx.doi.org/10.1016/j.jcsr.2014.04.014.